Journal of Inflammation Research

Dovepress
Taylor & Francis Group

Open Access Full Text Article

ORIGINAL RESEARCH

Molecular Mechanisms in Idiopathic Mitral Valve Chordae Tendineae Rupture: Insights from Transcriptome Analysis and Inflammation Evaluation

Qiuji Wang[1–3,*], Lishan Zhong[1,2,*], Linbin Hua[1–3], Shanwen Pang[1–3], Yuxin Li[1,2], Zhaolong Zhang[1,2], Junfei Zhao[1,2], Huanlei Huang[1–3]

[1]Department of Cardiac Surgery, Guangdong Provincial People's Hospital (Guangdong Academy of Medical Sciences), Southern Medical University, Guangzhou, 510080, People's Republic of China; [2]Guangdong Cardiovascular Institute, Guangzhou, 510030, People's Republic of China; [3]Guangdong Provincial Key Laboratory of South China Structural Heart Disease, Guangzhou, People's Republic of China

*These authors contributed equally to this work

Correspondence: Huanlei Huang; Junfei Zhao, Department of Cardiac Surgery, Guangdong Provincial People's Hospital (Guangdong Academy of Medical Sciences), Southern Medical University, 106 Zhongshan Second Road, Yuexiu District, Guangzhou, Guangdong, People's Republic of China, Email hhuanlei@hotmail.com; zhaojunfei@gdph.org.cn

Objective: This study investigates the molecular mechanisms and hub genes in idiopathic rupture of mitral valve chordae tendineae (iRCT).

Methods: Histological changes were assessed via pathological staining, and transcriptome sequencing was performed on samples from 8 iRCT patients and 6 controls. Differentially expressed genes (DEGs), functional enrichment, PPI networks, and immune cell infiltration were analyzed. Hub gene expression was validated using RT-qPCR.

Results: iRCT samples exhibited cell proliferation, disorganized collagen fibers, and elastin fiber rupture. Immunohistochemical analysis further confirmed that activated fibroblasts, macrophages, dendritic cells, and T cells were increased in iRCT samples compared to normal samples. Additionally, iRCT samples exhibited an increased content of collagen fibers and elastin fibers. Transcriptome analysis identified 208 DEGs (109 upregulated, 99 downregulated) linked to inflammation, immune activation, and extracellular matrix remodeling.

Conclusion: iRCT involves ECM remodeling, inflammation, and immune dysregulation, with identified hub genes offering potential therapeutic targets.

Keywords: mitral valve prolapse, chordae tendineae rupture, inflammation, immune response, transcriptome, bioinformatics

Introduction

The chordae tendineae connect the mitral valves to the papillary muscles. Along with the mitral annulus, mitral leaflets, and papillary muscles, the chordae tendineae form the complete mitral apparatus. This apparatus coordinates during the cardiac cycle to prevent mitral leaflet prolapse into the atrium and to ensure unidirectional blood flow from the left atrium to the left ventricle.[1]

Rupture of chordae tendineae (RCT) is a primary cause of mitral regurgitation (MR), leading to severe hemodynamic changes and potentially acute congestive heart failure.[2] RCT can be classified based on its etiology: approximately 24.4% of cases are secondary RCT, with clear causes such as rheumatic heart disease, infective endocarditis, and ischemic cardiomyopathy. About 74.6% of cases are idiopathic RCT (iRCT) with unknown causes, commonly observed in fibroelastic deficiency (FED) mitral valve prolapse (MVP), and are most likely to occur in the P2 region of the posterior leaflet.[3–5] iRCT is common in older individuals and is generally associated with age-related connective tissue

Received: 20 December 2024
Accepted: 29 March 2025
Published: 5 April 2025

degeneration.[6] However, we found iRCT in young FED patients, suggesting that factors other than degenerative changes contribute to its occurrence. Some studies have linked the iRCT phenotype to inflammatory responses, abnormal mechanical traction, and other factors identified through pathological examination and computer simulations.[7–9] However, the specific mechanisms that cause iRCT are still unclear.

The current primary treatment for MR caused by iRCT involves replacing the ruptured chordae tendineae with artificial chordae. However, because pathogenic factors persist, patients may experience recurrent MR after surgery due to the rupture of other seemingly "normal" chordae tendineae.

This study aims to identify the pathogenic genes and mechanisms involved in iRCT through transcriptome sequencing. This will provide insights into the diagnosis and treatment of iRCT, enabling more targeted, precise treatments and reducing its incidence.

Methods

Collection of Chordae Tendineae Samples and Transcriptome Sequencing

Eight iRCT samples were collected from the P2 region of the posterior leaflet, the most commonly affected area in iRCT, at the department of cardiac surgery, Guangdong Provincial People's Hospital, in 2023. All iRCT patients were sporadic cases, with no history of syndromic disorders such as Marfan syndrome, Loeys–Dietz syndrome, or other connective tissue diseases. All iRCT patients underwent mitral valvuloplasty under cardiopulmonary bypass, and the iRCT samples were collected from the margin of the prolapsed leaflet. Normal chordae tendineae samples were obtained from heart transplant recipients with no valvular heart disease. A total of 14 samples (8 iRCT and 6 normal) were selected for whole transcriptome sequencing.

Total RNA was extracted from each sample using TRIzol Reagent (Thermo Fisher, USA). Sequencing was performed by Jikai Gene Chemical Technology Co., Ltd. (Shanghai, China). RNA libraries were constructed using the NEBNext® UltraTM RNA Library Prep Kit for Illumina® (NEB, USA), following the manufacturer's instructions. The library products were sequenced on the Illumina Novaseq platform, generating no fewer than 10 million paired-end reads per sample. Raw reads were trimmed for adapter sequences, filtered for low-complexity or low-quality sequences, and mapped to the hg38 genome using Hisat2 (version 2.1.0).[10]

This study was conducted in accordance with the Declaration of Helsinki and approved by the Ethics Review Committee of Guangdong Provincial People's Hospital (KY2023-256-02). Informed consent was obtained from all participants.

Identification of Differentially Expressed Genes

Differentially expressed genes (DEGs) between iRCT and normal samples were identified using the DESeq2 package (version 3.11.0)[11] in R software (version 3.6.1). The Benjamini and Hochberg-corrected p value of < 0.05 and $|\mathrm{Log_2}^{\mathrm{Fold\ Change}}| > 1$ were defined as the selection thresholds for selecting the DEGs.

Gene Function Enrichment Analysis

Gene Set Enrichment Analysis (GSEA) (http://www.gsea-msigdb.org/) was performed for all genes, and GSEA pathway enrichment maps were generated. Gene Ontology (GO), Kyoto Encyclopedia of Genes and Genomes (KEGG), and REACTOME signaling pathways were analyzed for upregulated and downregulated DEGs and visualized on the SRplot web server (https://www.bioinformatics.com.cn/srplot).

PPI Network and Modular Analysis

A PPI network for upregulated and downregulated DEGs was constructed using the STRING database (version 12.0),[12] and visualized with Cytoscape software (version 3.10.2).[13] The Cytoscape plugin MCODE was used to identify key functional modules in all DEGs (parameters: degree cutoff = 2, node score cutoff = 0.2, K-core = 2, and max depth = 100). The plugins Cytohubba and CytoNCA were used to detect hub genes in upregulated and downregulated DEGs separately.

Identification of IRDEGs and Immune Cell Infiltration Analysis

A total of 1811 immune-related genes were identified from the Immunology Database and Analysis Portal (http://immport.niaid.nih.gov). The Venny 2.1.0 tool (https://bioinfogp.cnb.csic.es/tools/venny/index.html) was used to select 35 immune-related DEGs (IRDEGs). Immune cell infiltration was estimated using transcriptome sequencing data and the ImmuCellAI.[14]

Validation of Hub Genes

Nine normal and nine iRCT samples, not used for transcriptome sequencing, were selected to validate hub genes' expression level. Total RNA was extracted from each sample using an RNA extraction kit (EZBioscience B0004D, China). First-strand cDNA synthesis was performed using a reverse transcription kit (EZBioscience A0010CGQ, China). SYBR Green real-time quantitative PCR kit (EZBioscience A0012-R2, China) was used for real-time quantitative polymerase chain reaction (RT-qPCR) on a qTower3 G Touch (Analytik Jena, Jena, Germany). β-Actin was used as a control.

Histopathological Examination

Tissue samples were fixed in 4% neutral buffered formalin overnight at room temperature. After fixation, samples were sequentially dehydrated with increasing concentrations of ethanol (70%, 80%, 95%, and 100%), cleared in xylene, and then embedded in paraffin. 5 μm-thick paraffin sections were prepared for histopathological examination. Hematoxylin-eosin (HE) staining was performed using an HE Staining kit (Solarbio G1120, China) according to the manufacturer's instructions. Masson's trichrome staining was performed using a standard protocol (Beyotime C0189S, China) to differentiate collagen fibers from other extracellular matrix components. Elastic Van Gieson (EVG) staining (ZSGB-BIO BSBA-4083B, China) was performed by incubating sections with elastic fiber-specific solutions, followed by counterstaining with Van Gieson stain to highlight collagen and elastic fibers. All stained sections were examined under light microscopy to assess histological features, including collagen deposition and elastic fiber integrity.

Immunohistochemical staining was performed to localize immune cells in the tissue samples. Paraffin-embedded sections (5 μm thick) were deparaffinized, rehydrated, and subjected to antigen retrieval using citrate buffer (pH 6.0) at 95°C for 20 minutes. After cooling, sections were blocked with 5% bovine serum albumin (BSA) for 1 hour at room temperature. Primary antibodies against α-SMA (Fibroblast marker, Abcam, #ab7817), CD3 (T-cell marker, Abcam, #ab5690), CD11c (dendritic cell marker, Abcam, #ab52632), CD45 (pan-leukocyte marker, Abcam, #ab10558), and CD68 (macrophage marker, Abcam, #ab955) were applied at 1:100 dilution and incubated overnight at 4°C. Sections were then incubated with HRP-conjugated secondary antibodies for 30 minutes at room temperature. Immunoreactivity was visualized using a DAB substrate kit (Vector Laboratories, #SK-4100). Slides were counterstained with hematoxylin, dehydrated, and mounted. Immunohistochemical images were captured from three randomly selected random regions of interest (ROIs) per sample at 40× magnification. The positively stained area was measured and normalized to the total tissue area within the ROI. The mean percentage of positive area was calculated for each sample and used for statistical analysis.

Color deconvolution was performed using ImageJ software with the "Color Deconvolution" plugin. The plugin was calibrated for Masson trichrome and EVG stains to isolate collagen, elastic fibers, and cytoplasmic elements. The resulting images were analyzed to calculate the relative area percentage of each constituent. Three ROIs (40×) were selected from each image for quantification to ensure statistical reliability.

Statistical Analysis

Continuous variables with a normal distribution were expressed as the mean ± standard deviation, and group comparisons were performed using the independent samples *t*-test. Non-normally distributed continuous variables were expressed as the median and interquartile range, with comparisons between groups performed using the Mann–Whitney *U*-test. A p-value < 0.05 was considered statistically significant. Data were analyzed using GraphPad Prism 10.0 software. Spearman correlation was used to explore the relationship between key regulators and immune cell infiltration levels, as well as IRDEG expression.

Results

Overall Protocol of the Study

The flowchart of our study is shown in Figure 1.

Morphological Features of iRCT and Normal Samples

Histological staining revealed significant cellular proliferation in the subepithelial layer and dense collagenous core of the iRCT samples, with markedly increased cell density, accompanied by an increase in activated fibroblasts (Figures 2 and S1A). The cells in the iRCT samples lost the uniform distribution seen in normal chordae tendineae. EVG staining confirmed that elastic fibers in both normal chordae tendineae and the unruptured ends of iRCT samples were primarily located in the subendothelial layer, arranged in a uniform linear pattern. However, at the ruptured ends of the iRCT samples, abnormal proliferation of elastic fibers was observed, accompanied by a loss of the orderly linear structure. Instead, short, wavy elastic fiber bundles infiltrated the dense collagen core. Masson's trichrome staining demonstrated that collagen fibers in normal chordae tendineae were well-aligned and organized. In contrast, disorganized collagen fibers and ruptured collagen bundles were observed at both the ruptured and unruptured ends of the iRCT samples. These findings suggest that even the unruptured chordae in iRCT samples exhibit pathological alterations and should not be considered entirely normal.

Color deconvolution was used to quantify collagen and elastic fibers in the histological images of ruptured and normal chordae tendineae. The area occupied by each component was expressed as a percentage of the total tissue area. For elastic fibers, the analysis revealed significantly reduced content in the normal group (2.95% ± 1.44%) compared to the iRCT group (26.71% ± 8.23%, $p < 0.01$). In contrast, collagen fibers were significantly increased in the iRCT group (75.53% ± 8.15%) compared to the normal group (47.44% ± 12.43%, $p < 0.01$) (Figure S1B).

Immunohistochemical analysis revealed a marked increase in immune cell infiltration in iRCT tissues compared to normal samples. CD3-positive T cells were sparsely present in normal tissues but significantly enriched in iRCT samples,

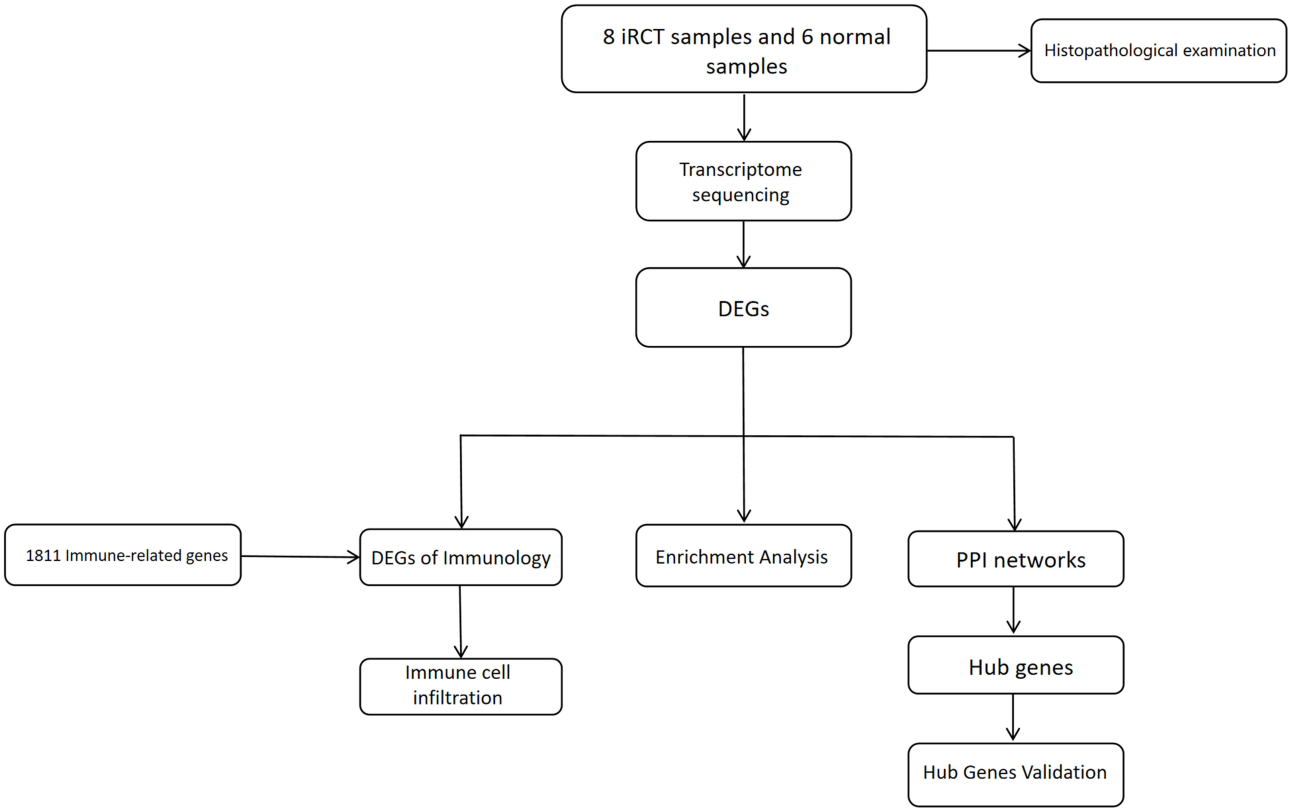

Figure 1 Overall protocol of the study.
Abbreviations: iRCT, idiopathic rupture chordae tendineae; PPI, protein-protein interaction; DEGs, differentially expressed genes.

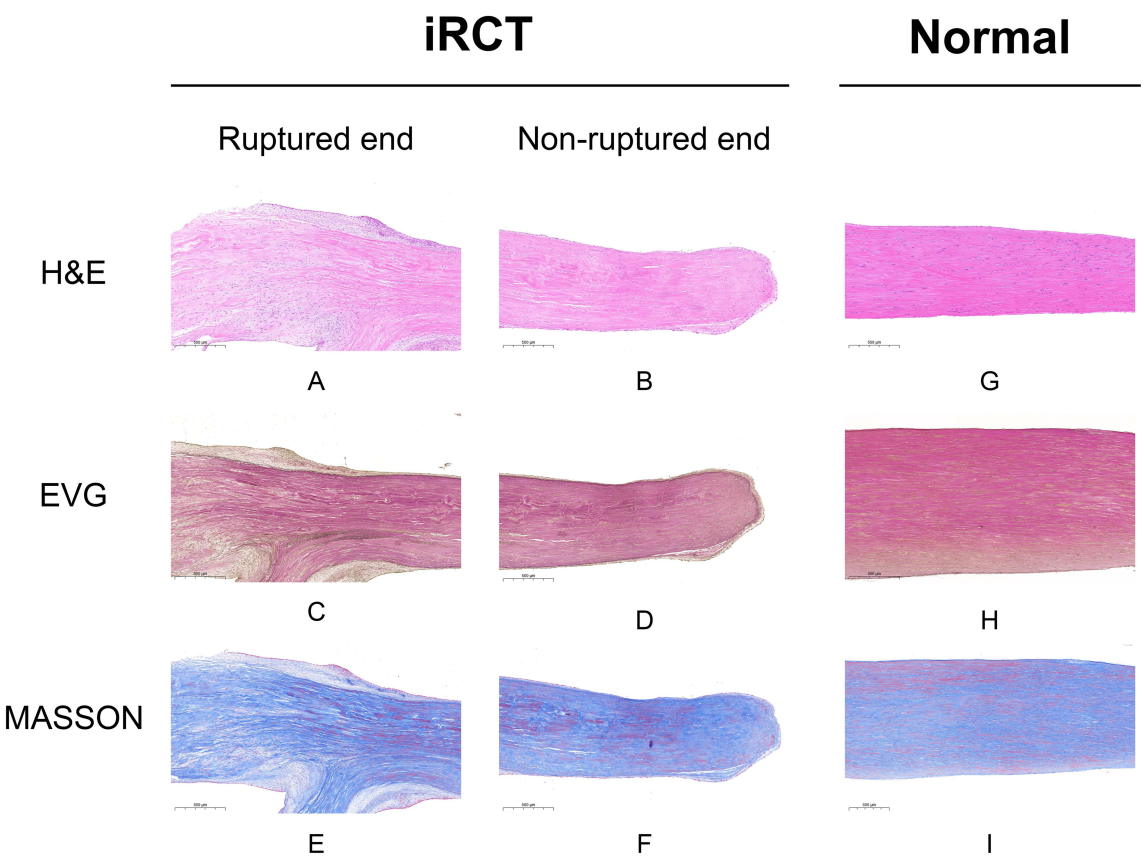

Figure 2 Morphological features of iRCT and normal sample. iRCT sample (**A–F**) and normal sample (**G–I**) were stained for H&E (**A, B** and **G**), elastin (**C, D** and **H**) and collagen (blue) (**E, F** and **I**). Scale bar = 500 um.

particularly within areas of collagen disruption. Similarly, CD11c-positive dendritic cells and CD68-positive macrophages showed significantly higher density in iRCT tissues, correlating with regions of elastic fiber degradation and ECM disorganization (Figure S2).

Identification of Differentially Expressed Genes

A total of 208 DEGs were identified, of which 109 were upregulated and 99 downregulated (Figure 3A). The heatmap of DEGs expression showed a clear distinction in mRNA levels between the iRCT and normal samples (Figure 3B).

Gene Function Enrichment Analysis

To explore the functions of differentially expressed genes and their associated pathways, we performed GSEA. We found significant enrichment in inflammatory processes and extracellular matrix (ECM) components. KEGG pathway analysis suggested that DEGs were associated with inflammatory responses, immune cell activation, and autoimmune disease pathways (Figure 3C, D, and Tables S1–S3).

We further analyzed the functions of the upregulated and downregulated DEGs. In the BP component, upregulated DEGs were primarily enriched in cell adhesion, while downregulated DEGs were mainly involved in immune response. In the CC category, the DEGs were mainly enriched in the extracellular matrix and cell membrane. In the MF component, downregulated DEGs were primarily enriched in calcium ion binding, while upregulated DEGs were enriched in signaling receptor binding (Figure 3E–G). REACTOME pathway analysis revealed that upregulated DEGs were enriched in GPCR signaling, cytokine signaling in the immune system, and extracellular matrix organization, while downregulated DEGs were primarily enriched in immune system pathways (Figure 3H). Many of these pathways are involved in ECM organization and regulation of inflammatory or immune responses.

https://doi.org/10.2147/JIR.S510525

https://doi.org/10.2147/JIR.S510525

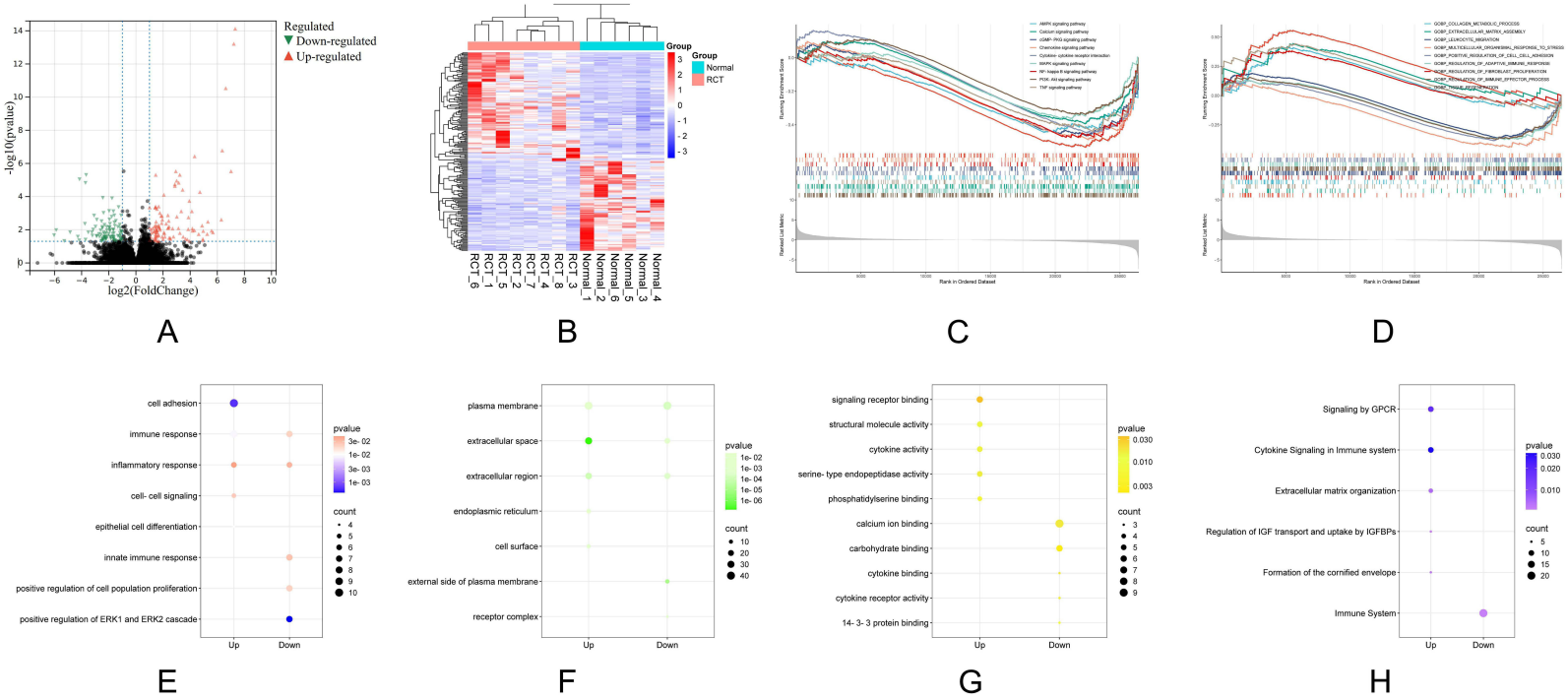

Figure 3 Identification of differentially expressed genes (DEGs) and Gene Function Enrichment analysis. (**A**) Volcano plot of DEGs; red indicates up-regulate genes; green indicates down-regulated genes. (**B**) Heatmap showing the expression of DEGs. (**C**) GSEA enrichment analysis of biological process. (**D**) GSEA enrichment analysis of KEGG. (**E**) GO-BP enrichment analysis of DEGs. (**F**) GO-CC enrichment analysis of DEGs. (**G**) GO-MF enrichment analysis of DEGs. (**H**) REACTOME pathways enrichment analysis of DEGs.

PPI Network and Modular Analysis

Figure 4A shown the identification of the biggest functional modules, consisting of 10 DEGs: CD1E, FN1, SDC1, KRT17, CEACAM1, KRT14, CXCR6, CD69, CTLA4, and CD1C, using the MCODE plugin in Cytoscape. To validate the expression of these genes, RT-qPCR was performed on a new cohort of nine normal and nine iRCT samples. RT-qPCR results strongly correlated with those from transcriptome sequencing, except for KRT14 (Figure S3). Hub genes were identified using Cytohubba and CytoNCA, with genes ranked based on their scores. FN1, KRT14, KRT17, LAMB3, PKP1, KRT16, DLX3, THY1, PLAU, and BDKRB2 were designated as upregulated hub genes (Figure 4B and C), while CD69, CTLA4, PDCD1, CCL19, TIGIT, CEACAM1, CXCR6, CD1C, RGS1, and DUSP2 were identified as downregulated hub genes (Figure 4D and E). Upregulated hub genes were mainly associated with structural integrity, tissue remodeling, wound healing, and cellular adhesion, while downregulated hub genes were primarily involved in immune regulation, lymphocyte activation, and inflammation.

Immune Cell Infiltration Analysis

Our enrichment analyses revealed significant enrichment of DEGs in pathways related to inflammation and immune response. To investigate the impact of immune infiltration in iRCT, we used the ImmuCellAI algorithm. This enabled us to assess the relationship between IRDEGs and immune infiltration in iRCT samples. Our analysis identified 35 immune-related differentially expressed genes (IRDEGs) from the datasets (Figure 5B and Table S4). Of the 24 immune cell types analyzed, seven showed significant differences in iRCT samples compared to normal tissues (Figure 5A). Additionally, as shown in Figure 5B and C, we assessed the correlation between immune cells and IRDEGs/immune cells to explore their potential interactions. Figure 5B shown that SDC1 was strongly positively correlated with macrophages and negatively correlated with NK cells. CTLA4 exhibit a strong negative correlation with dendritic cells. Several IRDEGs, including CD1C, CD1E, and PTH1R, were associated with various T cell subtypes. Figure 5C illustrated that during iRCT, the strongest correlation was observed between macrophages and NK cells, and close interactions occur between various T cell subtypes.

Discussion

iRCT is not uncommon, with studies showing that 47.2% of MVP patients are affected.[15] iRCT causes paradoxical motion of the mitral valve leaflets during both systole and diastole, making it one of the most common causes of MR. Chronic MR leads to significant cardiac structural remodeling and impaired function, ultimately resulting in heart failure. Ling et al reported that medical treatments do not effectively alleviate iRCT-induced heart failure, with mortality rates significantly higher than expected.[16] Common surgical approaches include replacing ruptured chordae with artificial ones during cardiopulmonary bypass or off-pump surgery. However, since the underlying cause of iRCT remains unaddressed, patients may experience recurrent MR due to rupture of seemingly "normal" chordae.[17] In fact, the dense collagenous core of these seemingly normal chordae may have detached from the spongiosa and appeared ruptured and retracted before the initial surgery,[8] as confirmed by our pathological examination. Post-surgical changes in chordal tension may further contribute to the rupture of these seemingly "normal" chordae, leading to recurrent MR.

Current research on iRCT primarily focuses on phenotypic changes of ruptured chordae, while the specific underlying mechanisms remain unclear.[1,18] Molecular pathological studies are essential to explore potential therapeutic and preventive strategies for iRCT. Given the lack of transcriptomic studies on iRCT, we performed whole transcriptome sequencing on iRCT samples and compared them to sequencing data from healthy individuals.

Our enrichment analysis revealed that iRCT is strongly associated with inflammatory responses, immune reactions, cell proliferation, and cell-cell adhesion, all of which are integral to ECM organization. Through the construction of a PPI network, we identified both upregulated and downregulated hub genes in iRCT. In the PPI network of upregulated genes, several genes interact to form a cohesive network that plays a central role in ECM remodeling and tissue repair. FN1 contributes synergistically to tissue restoration, cell adhesion, and structural stability by interacting with keratins and other ECM proteins.[19,20] These interactions suggest that upregulated genes are essential for promoting tissue repair, cell migration, and the restoration of damaged areas. Specifically, interactions between FN1, KRT14, and KRT17 likely play a pivotal role in strengthening tissue structure and promoting cell recovery. Additionally, genes such as LAMB3 and

https://doi.org/10.2147/JIR.S510525

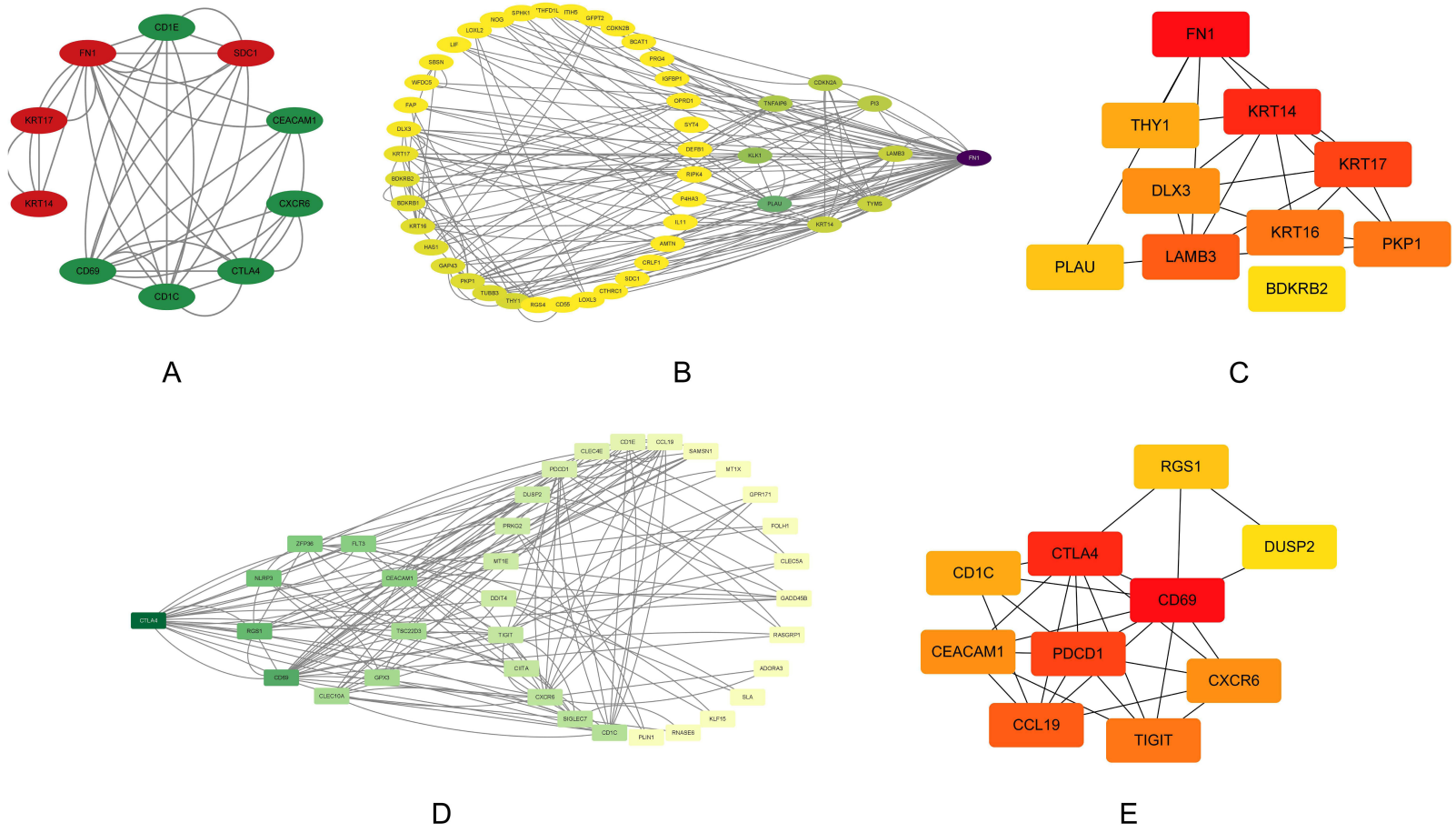

Figure 4 (**A**) Main functional modules in all DEGs were analysed by MCODE. Red genes are up-regulated DEGs and green genes are down-regulated DEGs. (**B** and **C**) Hub genes of up-regulated DEGs were analysed by cytoNCA and cytoHubba, separately. (**D** and **E**) Hub genes of up-regulated DEGs were analysed by cytoNCA and cytoHubba, separately. The darker the gene, the higher the score.

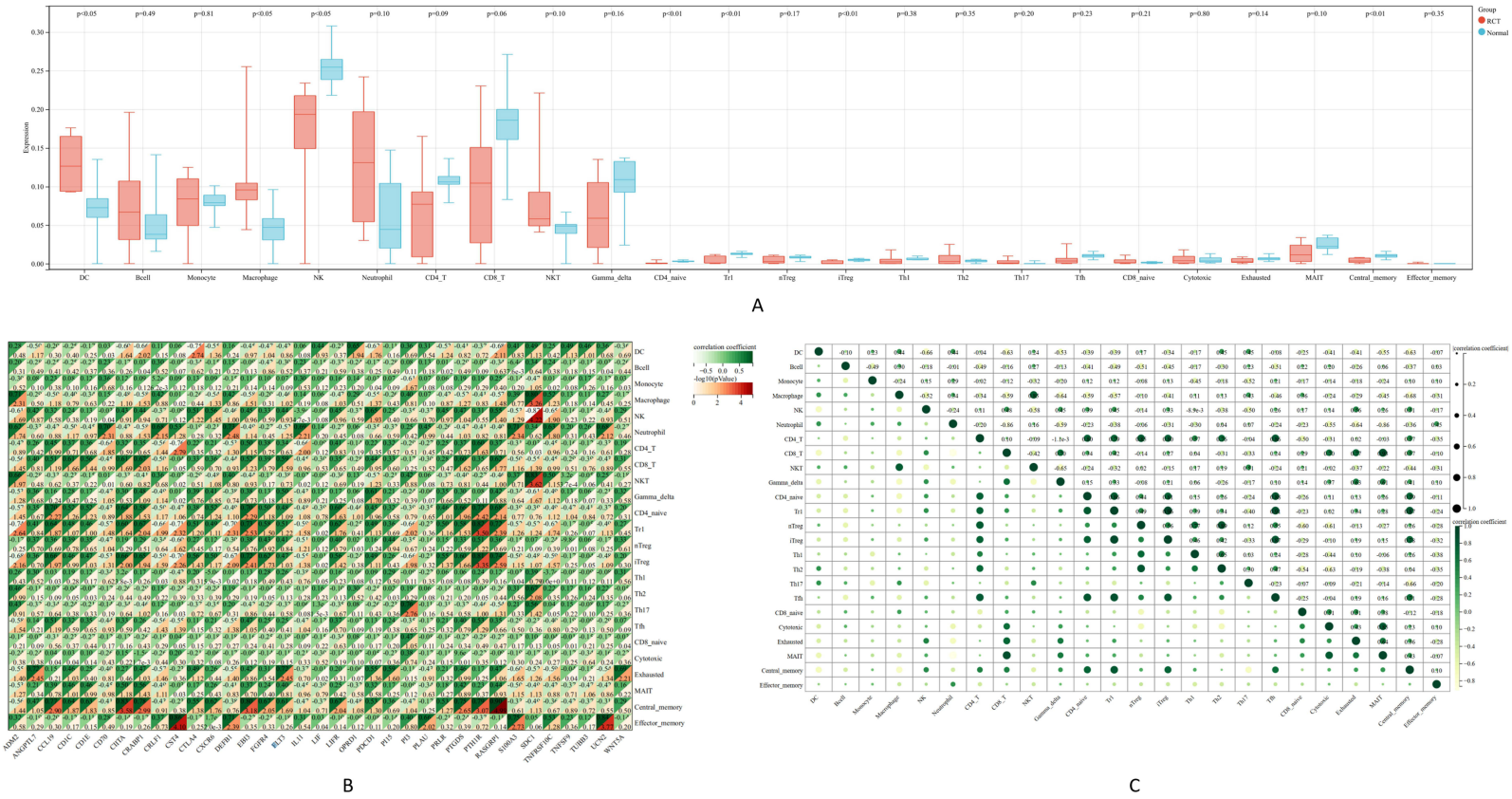

Figure 5 (**A**) Differential expression of immune cells between the two groups. (**B**) correlation between immune cells and IRDEGs. (**C**) Correlations between immune cells.

PKP1 stabilize the connection between cells and the basement membrane, while DLX3 and THY1 regulate cell differentiation and immune responses, further driving tissue remodeling.[21–24] Collectively, through their coordinated actions, these upregulated genes influence ECM stability, cellular repair mechanisms, and immune responses, facilitating the repair process in iRCT. In contrast, the downregulation of immune-related genes such as CTLA4 and CD69 could lead to immune system dysregulation, enhancing immune cell activation and inflammatory responses, which exacerbates tissue damage. Specifically, downregulation of CTLA4 and upregulation of CD69 may result in excessive immune activation, while the downregulation of PDCD1 and TIGIT further disrupts immune tolerance, causing sustained immune responses.[25,26] Moreover, the downregulation of chemokines like CCL19 and CXCR6 may impair the directed migration of immune cells and their regulation in inflammatory areas, intensifying local immune dysregulation.[27] The downregulation of RGS1 and DUSP2 may disrupt immune signaling, leading to immune response dysfunction and further contributing to immune-mediated tissue damage and degradation in iRCT.[28,29] These interactions among downregulated genes highlight the strong connection between immune system dysregulation and tissue damage, suggesting that immune regulatory pathways play a crucial role in the pathogenesis of iRCT.

Our pathological staining results show that normal mitral valve chordae tendineae consist of uniformly distributed collagen and elastin fibers arranged in a linear pattern beneath the epithelium. These fibers are critical for maintaining the strength and elasticity of the chordae tendineae. In iRCT, however, immune imbalance and localized inflammation disrupt the stability of these fibers, affecting ECM synthesis and degradation. Our findings indicate that 35 IRDEGs play critical roles in iRCT. For instance, CCL19, CXCR6, and CD70 activate fibroblasts and immune cells, promoting the secretion of collagenases and elastases, which accelerate collagen and elastin fiber degradation.[26,30–33] Additionally, abnormal expression of CTLA4, PDCD1, and TIGIT may lead to sustained inflammation, disrupting ECM turnover and contributing to chordal tendineae structural damage.[34,35]

The ECM serves as a critical structural scaffold for mitral valve chordae tendineae, and its integrity is vital for maintaining chordal function.[36] Significant changes in ECM components were observed in iRCT patients. IRDEGs like CRLF1, CRABP1, and SDC1 play key roles in ECM regulation and matrix metalloproteinase recruitment, degrading collagen and elastin fibers, leading to tissue weakening and rupture.[37] Furthermore, IRDEGs such as TNFRSF10C, TNFSF9, and PTH1R regulate apoptosis and fibroblast turnover, influencing the balance of ECM synthesis and degradation.[38] Figure 5B and C present our immune cell infiltration analysis, providing valuable insights into the immune landscape of iRCT. SDC1 shows a strong positive correlation with macrophages and a negative correlation with NK cells, suggesting its pivotal role in macrophage activation and immune modulation in iRCT. In contrast, CTLA4 is negatively correlated with dendritic cells, suggesting its role in regulating immune responses at the level of antigen-presenting cells. Furthermore, several IRDEGs, including CD1C, CD1E, and PTH1R, are associated with various T cell subtypes, emphasizing the complexity of T cell involvement in iRCT. Notably, Figure 5C shows that macrophages and NK cells have the strongest correlation, possibly reflecting an immune response that drives ECM remodeling and tissue damage in iRCT. Additionally, the close interactions among various T cell subtypes further suggest a coordinated immune response, contributing to the chronic inflammatory environment characteristic of iRCT. These findings offer a comprehensive view of immune dysregulation in iRCT, shedding light on the inflammatory processes that drive tissue damage and remodeling. Further research is needed to elucidate the functional roles of these immune interactions and their potential as therapeutic targets in iRCT.

The immunohistochemical findings confirm a strong immune component in iRCT pathogenesis, as indicated by increased infiltration of CD3-positive T cells, CD11c-positive dendritic cells, and CD68-positive macrophages. These immune cells likely contribute to the localized inflammation and ECM degradation observed in iRCT tissues. Increased macrophage presence suggests active tissue remodeling, as macrophages are key mediators of collagenase and elastase secretion, facilitating ECM breakdown.[39] The enrichment of dendritic cells may indicate ongoing antigen presentation and immune activation, further perpetuating inflammation.[40] Together, these results highlight the interplay between immune cell infiltration, inflammation, and ECM degradation in iRCT, suggesting potential therapeutic targets to mitigate immune-mediated damage in these tissues. These findings provide a comprehensive view of the immune dysregulation in iRCT, with implications for understanding the inflammatory processes that drive tissue damage and remodeling. Further

studies are needed to elucidate the functional roles of these immune interactions and their potential as therapeutic targets in iRCT.

Previous studies show that during iRCT, fibroblasts are excessively activated into myofibroblasts, characterized by heightened proliferation and ECM overproduction.[4,41,42] This finding aligns with our pathological observations. Increased fibroblast proliferation, coupled with ECM integrity loss, forms a vicious cycle that exacerbates inflammation and tissue damage, accelerating degenerative changes in chordae tendineae.[43–45] This cycle is driven by continuous inflammatory pathway activation, fibroblast proliferation, and ongoing ECM degradation, ultimately leading to iRCT.

Traditionally, iRCT research has focused on the immune response and ECM remodeling at the ruptured end. However, our study reveals that ECM disruption also occurs at the non-ruptured end, suggesting its potential role in the onset and progression of iRCT. The disruption of the ECM at the non-ruptured end may be closely associated with the pathological changes observed at the ruptured end. Although the non-ruptured end in iRCT patients does not experience obvious mechanical damage, studies indicate significant changes in ECM components, including collagen and elastin fibers. These alterations may cause structural instability in the tissue, thereby contributing to the pathological conditions that lead to iRCT. Although the immune response at the non-ruptured end may be less pronounced, ECM alterations could signal local cells, triggering immune cell recruitment and inflammatory responses. Additionally, the immune response at the non-ruptured end may differ from that at the ruptured end. While the ruptured end is generally regarded as the primary site of immune cell infiltration, the non-ruptured end may show distinct immune responses, especially in local immune regulation. Immune cells, such as macrophages and dendritic cells, may initially respond to ECM changes at the non-ruptured end, fostering a localized chronic inflammatory environment. This persistent inflammatory state may progressively impair tissue function, ultimately leading to chordae tendineae rupture over time. Therefore, a more detailed analysis of immune cell infiltration and ECM remodeling at the non-ruptured end would not only provide a deeper understanding of iRCT pathogenesis but also offer valuable insights for identifying potential therapeutic targets.

Our study identified several hub genes, such as CD1E, FN1, SDC1, KRT17, CEACAM1, KRT14, CXCR6, CD69, CTLA4, and CD1C, which, as described above, play important roles in immune responses, extracellular matrix remodeling, and tissue repair in iRCT. These genes, as potential therapeutic targets, regulate immune cell activation and migration, ECM stability, and tissue repair. Targeting these genes may provide new directions for the treatment of iRCT.

This study provides new insights into the pathogenesis of iRCT, though several limitations should be noted. First, the sample size is small, which may limit the generalizability of our findings. Larger studies are required to validate these results. Second, this study did not conduct a dynamic analysis of tissue samples at different stages of iRCT, so changes in gene expression during disease progression remain unclear. Furthermore, although transcriptome sequencing provided valuable insights into potential mechanisms, functional validation experiments are lacking, and the causal relationship between key genes and iRCT remains unconfirmed. Additionally, both ruptured and non-ruptured ends of the chordae tendineae were included in our analysis, which could introduce confounding factors. Although we initially considered using single-cell RNA sequencing, technical challenges related to small tissue size and insufficient cell yield prevented its application. Future studies utilizing Digital Spatial Profiling or similar technologies could overcome these limitations and provide cell-specific insights. Overall, our study offers important clues about the pathological mechanisms of iRCT, but further research combining multi-omics data and functional experiments is needed to fully elucidate these mechanisms.

In conclusion, this study provides novel insights into the molecular mechanisms underlying iRCT by utilizing transcriptome sequencing. Our findings suggest that inflammation, immune dysregulation, and ECM remodeling play central roles in the damage and rupture of mitral valve chordae tendineae.

Data Sharing Statement

The datasets generated during and analysed during the current study are available from the corresponding author on reasonable request.

Human Ethics Declaration

All procedures followed were in accordance with the ethical standards of the Ethics Review Committee of Guangdong Provincial People's Hospital on human experimentation and with the Helsinki Declaration of 1975, as revised in 2000 (5). Informed consent was obtained from all patients for being included in the study.

Acknowledgment

Huanlei Huang and Junfei Zhao are co-corresponding authors.

Funding

This work was supported by National Natural Science Foundation of China [grant numbers 82270373], the Clinical high-tech project of Guangzhou Municipal Health Commission [grant numbers FTJCZ0011] and the National Key Research and Development Program of China [grant numbers 2023YF2307003].

Disclosure

The authors report no conflicts of interest in this work.

References

1. Ross CJ, Zheng J, Ma L, Wu Y, Lee C. Mechanics and microstructure of the atrioventricular heart valve chordae tendineae: a review. *Bioengineering*. 2020;7(25):25. doi:10.3390/bioengineering7010025
2. Jeresaty RM, Edwards JE, Chawla SK. Mitral valve prolapse and ruptured chordae tendineae. *Am J Cardiol*. 1985;55:138–142. doi:10.1016/0002-9149(85)90315-7
3. Oliveira DB, Dawkins KD, Kay PH, Paneth M. Chordal rupture. I: aetiology and natural history. *Br Heart J*. 1983;50:312–317. doi:10.1136/hrt.50.4.312
4. Hjortnaes J, Keegan J, Bruneval P, et al. Comparative histopathological analysis of mitral valves in Barlow disease and fibroelastic deficiency. *Semin Thorac Cardiovasc Surg*. 2016;28:757–767. doi:10.1053/j.semtcvs.2016.08.015
5. Sedransk KL, Grande-Allen KJ, Vesely I. Failure mechanics of mitral valve chordae tendineae. *J Heart Valve Dis*. 2002;11:644–650.
6. van Wijngaarden AL, Kruithof BPT, Vinella T, Barge-Schaapveld DQCM, Ajmone Marsan N. Characterization of degenerative mitral valve disease: differences between fibroelastic deficiency and Barlow's disease. *J Cardiovasc Dev Dis*. 2021;8:23.
7. Kimura N, Shukunami C, Hakuno D, et al. Local tenomodulin absence, angiogenesis, and matrix metalloproteinase activation are associated with the rupture of the chordae tendineae cordis. *Circulation*. 2008;118:1737–1747.
8. Koda Y, Tsukube T, Hoshino M, Yagi N, Ishibashi-Ueda H, Okada K. Structural properties in ruptured mitral chordae tendineae measured by synchrotron-based X-ray phase computed tomography. *J Synchrotron Radiat*. 2023;30:995–1002. doi:10.1107/S1600577523005167
9. Icardo JM, Colvee E, Revuelta JM. Structural analysis of chordae tendineae in degenerative disease of the mitral valve. *Int J Cardiol*. 2013;167:1603–1609. doi:10.1016/j.ijcard.2012.04.092
10. Daehwan K, Ben L, Steven LS. HISAT: a fast spliced aligner with low memory requirements. *Nat Methods*. 2015;12:357–60.
11. Michael IL, Wolfgang H, Simon A. Moderated estimation of fold change and dispersion for RNA-seq data with DESeq2. *Genome Biol*. 2014;15.
12. Damian S, Annika LG, David L, et al. STRING v11: protein-protein association networks with increased coverage, supporting functional discovery in genome-wide experimental datasets. *Nucleic Acids Res*. 2018;47.
13. Paul S, Andrew M, Owen O, et al. Cytoscape: a software environment for integrated models of biomolecular interaction networks. *Genome Res*. 2003;13.
14. Miao YR, Zhang Q, Lei Q, et al. ImmuCellAI: a unique method for comprehensive T-cell subsets abundance prediction and its application in cancer immunotherapy. *Adv Sci*. 2020;7:1902880. doi:10.1002/advs.201902880
15. Yu HT, Moon J, Yang W, et al. High prevalence of unrecognized chordae tendineae rupture in mitral valve prolapse patients undergoing valve replacement surgery. *Can J Cardiol*. 2013;29:1643–1648. doi:10.1016/j.cjca.2013.09.002
16. Ling LH, Enriquez-Sarano M, Seward JB, et al. Clinical outcome of mitral regurgitation due to flail leaflet. *N Engl J Med*. 1996;335:1417–1423. doi:10.1056/NEJM199611073351902
17. Lee LS, Kwon MH, Cevasco M, et al. Postoperative recurrence of mitral regurgitation after annuloplasty for functional mitral regurgitation. *Ann Thorac Surg*. 2012;94(1211–1216):1216–1217.
18. Tessler I, Reshef N, Shpitzen S, Gilon D, Durst R. Mitral valve prolapse: from new mechanisms to diagnostic challenges. *Kardiol Pol*. 2022;80:891–896. doi:10.33963/KP.a2022.0147
19. Aladal M, You W, Huang R, et al. Insights into the implementation of Fibronectin 1 in the cartilage tissue engineering. *Biomed Pharmacother*. 2022;148(112782):112782. doi:10.1016/j.biopha.2022.112782
20. Sarma A. Biological importance and pharmaceutical significance of keratin: a review. *Int J Biol Macromol*. 2022;219:395–413. doi:10.1016/j.ijbiomac.2022.08.002
21. Jung SN, Lim HS, Liu L, et al. LAMB3 mediates metastatic tumor behavior in papillary thyroid cancer by regulating c-MET/Akt signals. *Sci Rep*. 2018;8:2718. doi:10.1038/s41598-018-21216-0
22. Li K, Wu R, Zhou M, Tong H, Luo KQ. Desmosomal proteins of DSC2 and PKP1 promote cancer cells survival and metastasis by increasing cluster formation in circulatory system. *Sci Adv*. 2021;7:eabg7265. doi:10.1126/sciadv.abg7265

23. Beanan MJ, Sargent TD. Regulation and function of Dlx3 in vertebrate development. *Dev Dyn*. 2000;218:545–553. doi:10.1002/1097-0177(2000)9999:9999<::AID-DVDY1026>3.0.CO;2-B
24. Hagood JS. Thy-1 as an integrator of diverse extracellular signals. *Front Cell Dev Biol*. 2019;7(26). doi:10.3389/fcell.2019.00026
25. Buchbinder EI, Desai A. CTLA-4 and PD-1 pathways: similarities, differences, and implications of their inhibition. *Am J Clin Oncol*. 2016;39:98–106. doi:10.1097/COC.0000000000000239
26. Meyiah A, Al-Harrasi A, Ur RN, Elkord E. Effect of boswellic acids on the expression of PD-1 and TIGIT immune checkpoints on activated human T cells. *Fitoterapia*. 2025;181:106401. doi:10.1016/j.fitote.2025.106401
27. Lu X, Wang Z, Ye D, et al. The role of CXC chemokines in cardiovascular diseases. *Front Pharmacol*. 2021;12:765768. doi:10.3389/fphar.2021.765768
28. Lu D, Liu L, Ji X, et al. The phosphatase DUSP2 controls the activity of the transcription activator STAT3 and regulates TH17 differentiation. *Nat Immunol*. 2015;16:1263–1273. doi:10.1038/ni.3278
29. Flynn AL, Gans J, Escobedo J, et al. RGS1 modulates autophagic and metabolic programs and is a critical mediator of human regulatory t cell function. *J Immunol*. 2023;211:1656–1668. doi:10.4049/jimmunol.2200402
30. Onder L, Papadopoulou C, Lütge A, et al. Fibroblastic reticular cells generate protective intratumoral T cell environments in lung cancer. *Cell*. 2025;188:430–446. doi:10.1016/j.cell.2024.10.042
31. Tran-Nguyen TK, Xue J, Feghali-Bostwick C, Sciurba FC, Kass DJ, Duncan SR. CD70 activation decreases pulmonary fibroblast production of extracellular matrix proteins. *Am J Respir Cell mol Biol*. 2020;63:255–265. doi:10.1165/rcmb.2019-0450OC
32. Li CH, Xu LL, Zhao JX, et al. CXCL16 upregulates RANKL expression in rheumatoid arthritis synovial fibroblasts through the JAK2/STAT3 and p38/MAPK signaling pathway. *Inflamm Res*. 2016;65:193–202. doi:10.1007/s00011-015-0905-y
33. Chen PC, Deterding K, Engelskircher SA, et al. TIGIT-expression on natural killer cell subsets is an early indicator of alleviating liver inflammation following bulevirtide treatment in chronic hepatitis D. *Hepatology*. 2025. doi:10.1097/HEP.0000000000001238
34. He Z, Glass MC, Venkatesan P, et al. Systemic inflammation and lymphocyte activation precede rheumatoid arthritis. *bioRxiv*. 2024.
35. Lei Z, Tang R, Wu Y, et al. TGF-β1 induces PD-1 expression in macrophages through SMAD3/STAT3 cooperative signaling in chronic inflammation. *JCI Insight*. 2024;9. doi:10.1172/jci.insight.165544
36. Martin M, Gillett K, Whittick P, Wells SM. New insights on the formation of the mitral valve chordae tendineae in fetal life. *J Cardiovasc Dev Dis*. 2024;11.
37. Le V, Mei L, Voyvodic PL, et al. Molecular tension in syndecan-1 is regulated by extracellular mechanical cues and fluidic shear stress. *Biomaterials*. 2021;275(120947). doi:10.1016/j.biomaterials.2021.120947
38. Behrmann A, Zhong D, Li L, et al. PTH/PTHrP receptor signaling restricts arterial fibrosis in diabetic LDLR(-/-) mice by inhibiting myocardin-related transcription factor relays. *Circ Res*. 2020;126:1363–1378. doi:10.1161/CIRCRESAHA.119.316141
39. Ghoubay D, Borderie M, Grieve K, et al. Corneal stromal stem cells restore transparency after N(2) injury in mice. *Stem Cells Transl Med*. 2020;9:917–935. doi:10.1002/sctm.19-0306
40. Sochocka M, Ochnik M, Sobczyński M, et al. New therapeutic targeting of alzheimer's disease with the potential use of proline-rich polypeptide complex to modulate an innate immune response - preliminary study. *J Neuroinflammation*. 2019;16(137). doi:10.1186/s12974-019-1520-6
41. Goodwin RL, Kheradvar A, Norris RA, Price RL, Potts JD. Collagen fibrillogenesis in the mitral valve: it's a matter of compliance. *J Cardiovasc Dev Dis*. 2021;8:98. doi:10.3390/jcdd8080098
42. Lin T, Yang S, Chiu C, et al. Matrix metalloproteinase-1 mitral expression and −1607 1G/2G gene promoter polymorphism in mitral chordae tendinae rupture. *Transl Res*. 2013;161:406–413. doi:10.1016/j.trsl.2012.10.002
43. Rajlic S, Surmann L, Zimmermann P, et al. Fatty acid amide hydrolase deficiency is associated with deleterious cardiac effects after myocardial ischemia and reperfusion in mice. *Int J mol Sci*. 2022;23. doi:10.3390/ijms232012690
44. Yang L, Deng J, Ma W, et al. Ablation of lncRNA Miat attenuates pathological hypertrophy and heart failure. *Theranostics*. 2021;11:7995–8007. doi:10.7150/thno.50990
45. Pang H, Han B, Yu T, Zong Z. Effect of apelin on the cardiac hemodynamics in hypertensive rats with heart failure. *Int J mol Med*. 2014;34:756–764. doi:10.3892/ijmm.2014.1829